European Journal of Molecular & Clinical Medicine
ISSN 2515-8260 Volume 07, Issue 07 , 2021

AN AUTOMATED TONGUE COLOR IMAGE ANALYSIS FOR DISEASE DIAGNOSIS AND CLASSIFICATION USING DEEP LEARNING TECHNIQUES

[1]S. Rajakumaran, [2]Dr. J. Sasikala

[1]Research scholar, Dept. of Computer Science and Engineering, Annamalai University, Annamalai Nagar-608002.
[2]Research supervisor, Associate Professor, Dept. of Information Technology, Annamalai university, Annamalai Nagar-608002.
E-mail: srajakumaransubashini@gmail.com, sasikala.au@gmail.com

Abstract:

Tongue diagnosis is considered an effectual and non-invasive technique commonly used to carry out the secondary diagnosis at anytime and anywhere. Opportunely, computational models for image processing approaches in tongue are presented in the literature and obtained significant performance. Several tongue image analysis techniques are available, it is still needed to design an automated deep learning (DL) models for diagnosing the diseases through tongue image analysis. In this view, this paper devises a new automated DL based tongue color image analysis for disease diagnosis and classification. The presented technique makes use of distinct processes such as preprocessing, feature extraction, and classification. At the preprocessing stage, the presented model performsdata augmentation and gaussian filtering (GF) techniques for noise removal. Besides, the DL based Visual Geometry Group (VGG19), a convolutional neural network (CNN) model is applied to extract the useful set of feature vectors from the preprocessed image. In addition, the presented model utilizes two machine learning (ML) based classifiers such as random forest (RF) and gaussian naïve bayes (GNB) to perform classification processes. For theassessmentof the classification outcome of the presented technique, benchmark tongue image dataset is used. The experimental values pointed out that the presented VGG19-RF model has reached a higher precision, recall, accuracy, and F1-Score of 93.80%, 93.70%, 93.70%, and 93.68% respectively.

Keywords: Tongue color analysis, Deep learning, Machine learning, Feature extraction

1. Introduction:

Generally, human tongue is manufactured with abundant characteristics that are employed in disease diagnosing process and color features are one of the most vital objectives as defined in [1]. In traditional models, physicians investigate the color features by the prior knowledge in medical application. Unfortunately, uncertainty and subjectivity are often related to diagnostic outcomes. In order to eliminate the qualitative factors, tongue color analysis can be performed by using color features, which is a novel method for disease analysis, reduces the physical defection of patients when compared with alternate clinical examinations. Tongue image classification is defined as a major element in Traditional Chinese Medicine (TCM). In last decades, Chinese physicians have predicted the healthiness condition of a patient by the inspection of tongue's color, shape, and structure. Additionally, the

advancement in digital clinical imaging tools and pattern recognition models, computer aided tongue analysis is considered to be remarkable in TCM since the attained results are accurate, reliable, and objective medical analysis.

In last decades, tongue image feature extraction models are studied intensively. Based on the developed process, computer aided tongue analysis approaches are classified into 2 classes namely, single and multiple features. Numerous single feature extraction technologies were developed and utilized for tongue image diagnosis. These frameworks have applied useful data on simple descriptors like color, texture, shape, and orientation. As depicted, single feature is applied for examining the tongue images. In [2], proposed a color examination method of tongue images by gaining identical regions prior to perform classification process. Spectral Angle Mapper (SAM) examined and classified tongue colors under the application of spectral signatures instead of the color measures in RGB color space. In [3], researchers have concentrated on developing numerically defined tongue color space for prognostic feature extraction reliant on statistical distribution.

In [4], projected a feature extraction approach reliant on statistical characteristics. Despite developing several models, single feature was deployed with standard simulation outcomes, where it has employed low-level features. Thus, multi-features are applicable in predicting healthy and unhealthy tongue pictures. The studies have applied multi-features like integration of color and texture for finding and matching the tongue images. Some other models are also available in the literature [5, 6]. In [7], multi-labeled learning has been employed to classify tongue images based on the color and texture features. Obviously, the predefined models have employed low-level features where the properties of the tongue are not defined completely. Besides, it is essential to combine the model which is capable of generating full-set of features from tongue images.

The traditional works have defined and employed Deep Learning (DL) methods for the purpose of extracting high-level feature illustrations in extensive range of vision analyzing operations like handwritten digit prediction, face analysis, and object prediction. But only few studies have applied computer-aided tongue image analysis by applying DL approaches while computer-aided professional technique with reliability and objectivity and applied to serve as TCM and Western medical service. PCANet is assumed to a simpler Deep Neural Network (DNN) to classify images [8]. In principal componentanalysis network (PCANet) is compared with eminent and effective model Convolutional Neural Networks (CNN) by means of performance in different operations. Rather than using the weights of the network in CNN, updating them in backpropagation (BP) manner, PCANet can be treated as fundamental PCA filters for convolution filter banks in all phases with no future training. As PCANet was deployed, high-level extraction models are dependent on PCANet which is applied in face prediction, human fall analysis, speech emotion detection, etc. Even though PCANet is not employed in computer-aided tongue diagnoses, it is still comprised of various features which make it suitablefor tongue image categorization. As projected in PCANet, it can be simple to train and apply various data and processes with no adjustment in the system. Followed by, parameter fine-tuning should be added.

This paper devises a new automated DL based tongue color image analysis for disease diagnosis and classification. The presented technique makes use of distinct processes such as preprocessing, feature extraction, and classification. During the preprocessing stage, the presented model utilizes data augmentation toincreasethe size of the training dataset and Gaussian filtering (GF) technique for noise removal. Also, the DL based Visual Geometry

Group (VGG-19), a convolutional neural network (CNN) model is applied to extract the useful set of feature vectors from the preprocessed image. Along with that, the presented model utilizes two machine learning (ML) based classifiers such as random forest (RF) and gaussian naïve Bayes (GNB) to perform classification processes. For evaluating the classification results of the presented method, benchmark tongue image dataset is used.

2. The Proposed Model:

Fig. 1 displays the overall working operation of the presented model. As shown, the input images are preprocessed initially in two ways namely data augmentation and GF based noise removal. Then, the VGG-19 model gets executed to derive a useful set of feature vectors. Subsequently, the GNB and RF models are applied to categorize the distinct class labels of the applied test images. The detailed operation of these processes is discussed in the succeeding sections.

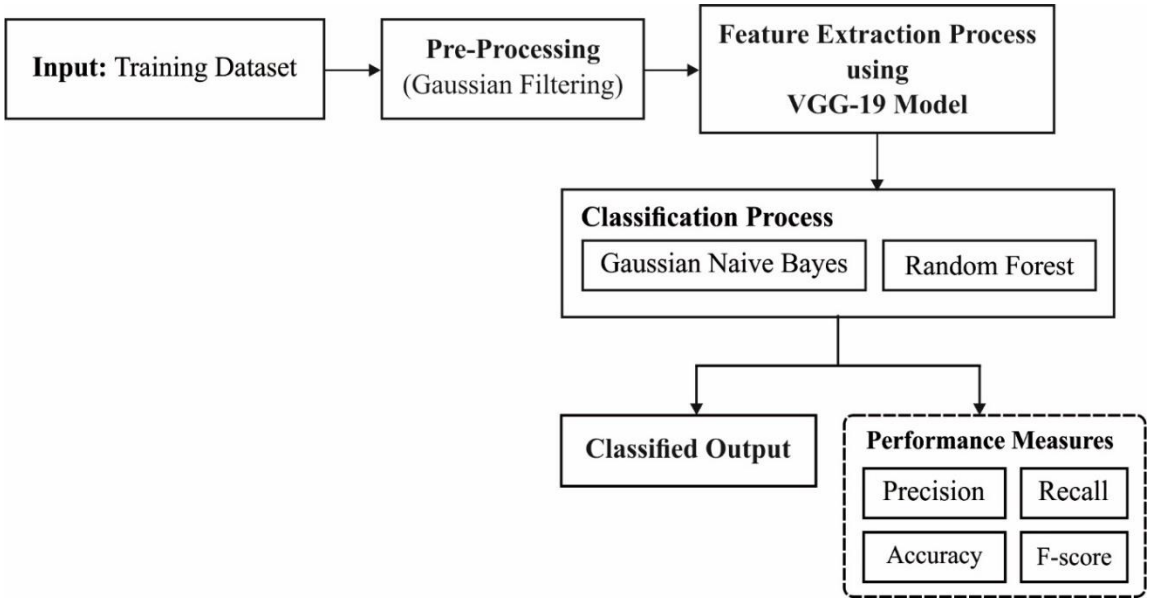

Fig. 1. Overall working process of proposed method

2.1. Image Preprocessing:

The image preprocessing takes place in 2 stages namely data augmentation and noise removal. Generally, the training of DL models necessitatesa massive quantity of the labeled data. The models which have undergone training data on limited dataset might result in degraded performance in some cases. The intolerable criteria of overfitting to the training data results in minimal outcome on the testing dataset. The process of enlarging the size of the dataset is a proficient way to minimize the overfitting or memorization issue. Simply, data augmentation is an artificial method of increase the data from the existing data to reduce overfitting problem. In this paper, data augmentation is performed with certain measures of rotationrange, zoomrange, widthshiftrange, heightshiftrange, shear range, horizontalflip,True, and fillmode. In Then, GF based noise elimination is computed.

There are different types of studies evolved in applications like astronomy, geography, and healthcare were applied prominently in digital image processing. Mostly the above-mentioned models require practical outcomes with better efficiency. The 2-D GF technique has been applied extensively for smoothing as well as noise elimination purposes. It demands

maximum processing resources and efficiency in implementation. The convolution operators are Gaussian operators which have been applied with the aim of Gaussian smoothing to be accomplished by convolution. Thus, the Gaussian operator in 1D is depicted by,

$$G_{1D}(x) = \frac{1}{\sqrt{2\pi}o} e^{-}\left(\frac{x^2}{2o^2}\right). \quad (1)$$

An optimal smoothing filter is placed in the spatial as well as frequency applications, which satisfies the uncertainty function as [9]:

$$\Delta x \Delta \boldsymbol{\omega} \geq \frac{1}{2}. \quad (2)$$

A Gaussian operator in 2D (circularly symmetric) is illustrated by,

$$G_{2D}(x,y) = \frac{1}{2\pi\sigma^2} e^{-}\left(\frac{x^2+y^2}{2\sigma^2}\right), \quad (3)$$

where σ (Sigma) implies a Standard Deviation (SD) of Gaussian function. When a maximum value is attained, then image smoothing effect becomes greater. (x,y) implies Cartesian coordinate points of the image that represent the dimension of a window. The GF is comprised of addition and multiplication operations among image and kernel, in which an image is illustrated by a matrix ranging between the values (8 bits). A kernel undergoes normalization of square matrix (0 and 1). A kernel is denoted by number of bits. In case of convolutional task, combination of a bit and a component of the image is divided by a power of 2.

The Mean Square Error (MSE) is a cumulative square error among the reconstructed image as well as actual image is illustrated as:

$$MSE = \frac{1}{M \times N}\sum_{i}\sum_{j}\left(O_{image} - R_{image}\right), \quad (4)$$

where $M \times N$ implies an Image size, $O_{image}$and R_{image}refers actual image and reconstructed image.

Peaksignaltonoise ratio (PSNR) is defined as a SNR is a ratio of feasible power of pixel value as well as power of distorted noise. Followed by, it also has impacted the actual image quality. It is described as:

$$PSNR = 10\log_{10}\left[\frac{255 \times 255}{MSE}\right], \quad (5)$$

where 255×255 defines a higher score of pixels and MSE is measured for actual as well as reformed image with $M \times N$ size. Therefore, it is essential to develop a productive logarithm multiplication unit for GF technique in order to compute practical simulation outcomes. Hence, an effective logarithm multiplier is applied to enhance the accuracy of GF technique.

2.2. Feature Extraction:

At this stage, the feature vectors in the pre-processed image are extracted by the use of VGG-19 model. CNN is a special type of Multilayer Perceptron (MLP), however, a simple NN is not suitable in learning complicated features, in contrast to DL structure. CNNs have exhibited tremendous function in various domains [10], like image classification, object prediction as well as clinical image detection. The major strategy behind CNN is to gain local features from high layer input and convert as low layers under massive features. The CNN is composed of convolution, pooling, and fully connected (FC) layers. The kernels convolve complete input by the use of "stride(s)" thus the dimensions of result are considered as integer values. Hence, the dimensions of input volume are reduced after using convolutional layer to implement the striding procedure. Moreover, zero padding is highly preferred to pad the input volume with zeros and retain input volume in conjunction with lowlevel features where the performance of convolutional layer is presented as:

$$F(i,j) = (I * K)(i,j) = \sum\sum I(i+m, j+n)\, K(m,n) \tag{6}$$

Where I denote input matrix, K implies a 2D filter of size m × n, and F indicates the result of 2D feature map. Also, performance of convolutional layer is projected by I*K. In order to enhance the non-linearity of feature map, Rectified Linear Unit (ReLU) layer has been employed. ReLU is applied to compute the activation by retaining the threshold input at 0. It is represented in numerical form as shown below:

$$f(x) = \max(0, x) \tag{7}$$

A pooling layer proceeds a down-sampling of applied input dimension which intends to mitigate the count of attributes. Also, FC layer is employed as a classification model which helps in making decision which depends upon the features attained from convolutional as well as pooling layers.

ConvNet Configuration					
A	A-LRN	B	C	D	E
11 weight layers	11 weight layers	13 weight layers	16 weight layers	16 weight layers	19 weight layers
input (224 × 224 RGB image)					
conv3-64	conv3-64 **LRN**	conv3-64 **conv3-64**	conv3-64 conv3-64	conv3-64 conv3-64	conv3-64 conv3-64
maxpool					
conv3-128	conv3-128	conv3-128 **conv3-128**	conv3-128 conv3-128	conv3-128 conv3-128	conv3-128 conv3-128
maxpool					
conv3-256 conv3-256	conv3-256 conv3-256	conv3-256 conv3-256	conv3-256 conv3-256 **conv1-256**	conv3-256 conv3-256 **conv3-256**	conv3-256 conv3-256 conv3-256 **conv3-256**
maxpool					
conv3-512 conv3-512	conv3-512 conv3-512	conv3-512 conv3-512	conv3-512 conv3-512 **conv1-512**	conv3-512 conv3-512 **conv3-512**	conv3-512 conv3-512 conv3-512 **conv3-512**
maxpool					
conv3-512 conv3-512	conv3-512 conv3-512	conv3-512 conv3-512	conv3-512 conv3-512 **conv1-512**	conv3-512 conv3-512 **conv3-512**	conv3-512 conv3-512 conv3-512 **conv3-512**
maxpool					
FC-4096					
FC-4096					
FC-1000					
soft-max					

Fig. 2. Structure of VGG-19

VGGNet is referred as a CNN with multi-layered process and depends upon the CNN approach and applied on ImageNet database. VGG-19 is applicable because of the simplicity and 3 × 3 convolution layers are enclosed to maximize a depth level. The volume size can be reduced using max pooling layers which act as a handler in VGG-19 [11]. The 2 FC layers are employed with 4096 neurons. In a training phase, convolution layers are utilized to feature extraction as well as max pooling layers related to convolution layers to limit the feature dimensionality. FC layers are utilized to make few feature vectors. Fig. 2 illustrates the structure of VGG-19 model [12].

2.3. Classification:

At last, the extracted feature vectors are fed into the GNB and RF models to identify the appropriate class labels of the input test images.

2.3.1. GNB Model:

The required strategy in Bayes model is considered to be a well-known priori and reduction of classification error possibility, correspondingly. A class-conditional density function is a popular and evaluated form of training dataset. In Bayesian evaluation, a training set is constrained with density function once the training set is upgraded and facilitated as observations to enable the transformation of a priori data as posterior density.The simple development has been invoked by means of 2 pattern classes namely, NAC and Placebo. In order to create simple numerical functions, then it is named as w_1 and w_2,correspondingly. Recalling a Bayes rule is considered to be,

$$P(w_i|x) = \frac{p(x|w_i)P(x_i)}{\sum_{i=1}^{2} p\,(x|w_i)P(w_i)}. \quad (8)$$

For a 2-class pattern w_1 and w_2, two Bayes classification rules have been adopted:

$$When\ P\ (w_1\ |x) > P(w_2\ |x)\ , x\ is\ allocated\ tow_1,$$

$$When\ P\ (w_1\ |x) < P(w_2\ |x)\ , x\ is\ allocated\ to\ w_2. \quad (9)$$

Assume the Gaussian Probability Distribution Function (PDF) along with μ_i as a mean value and Σj as a covariance matrix and resolved.

$$p(x|w_j) = \frac{1}{(2\pi)^{n/2|\Sigma_i|^{1/2}}}\ \exp\left(-\frac{1}{2}(x-\mu_i)^T\Sigma_i^{-1}(x-\mu_i)\right)\ \ i=\ 1,2. \quad (10)$$

By selecting a monotonic logarithmic differential function [13], the expression is defined as,

$$g_i(x) = -\frac{1}{2}(x-\mu_i)^T\Sigma_i^{-1}(x-\mu_i) +\ \ln P(w_i) \quad (11)$$

$-\frac{n}{2}\ \ln 2\pi - \frac{1}{2}\ \ln|\Sigma j|\ i = 1,2.$

Then, by evaluating the mean vector as well as covariance matrices for every class from training data and it is isolated by a hyperplane (symmetric covariance matrix) or hyper-quadrics (asymmetric covariance matrix).

2.3.2. RF Model:

In general, RF has defined the hybrid model developed by Breiman [14]. When the attained simulation is a discrete value, then it can be RF classification method, unlike it is a continuous value then it is a RF regression model. A massive number of empirical works have ensured that the RF method is composed of maximum prediction accuracy with remarkable tolerance for anomalous value. The RF classifier is applied in 2 states. Initially, RF model gains subsamples from actual samples with the help of bootstrap resampling module and makes Decision Trees (DT) for all samples. Secondly, a model divides the DT and executes a simple vote with classification as consequent result of detection. Hence, RF models are often evaluated with 3 phases namely,

(1) Decide the training data. Apply the bootstrap random sampling approach for retrieving K training sets from actual dataset (M properties), with a size of training set similar to actual training set.

(2) Develop the RF method. Make a classification regression tree to all bootstraps training sets in order to generate K- DTs to deploy a “forest”, but the newly developed trees are not pruned. In case of tree development, the model does not select optimal features as internal nodes which correspond branches [15]; however, branching task is applied as arbitrarydecision of m⩽M of features.

(3) Make simple voting.DT training is independent and training RF is computed in a parallel manner, which in turn enhances the performance efficiency. Therefore, RF is developed by

integrating K DTs significantly. When the input samples are classified, the simulation outcomes are reliant on simple voting of DT results.

3. Experimental Validation:

The simulation process of the presented model takes place using PC i5-8600k processor, GeForce 1050Ti, 4GB RAM, 16GB OS Storage, and 250GB SSD File Storage. The simulation tool used is Python 3.6.5 tool along with some packages namely tensorflow, keras, numpy, pickle, matplotlib, sklearn, pillow, and opencv-python. The performance validation takes place on a benchmark tongue dataset. The information related to the dataset is given in Table 1 and sample test images are depicted in Fig. 1. The results generated during the simulation process are displayed in Appendix. The dataset holds a set of 936 images with 78 images under distinct 12 class labels.

Table1: DatasetDescription

Diseases Name	**No. of Samples**
Chronic Kidney Disease	78
Nephritis	78
Verrucous Gastritis	78
Pneumonia	78
Nephritis Syndrome	78
Chronic Cerebral Circulation Insufficiency	78
Upper Respiratory Tract Infection	78
Erosive Gastritis	78
Coronary Heart Disease	78
Chronic Bronchitis	78
Mixed Hemorrhoid	78
Healthy	78
Total Images	**936**

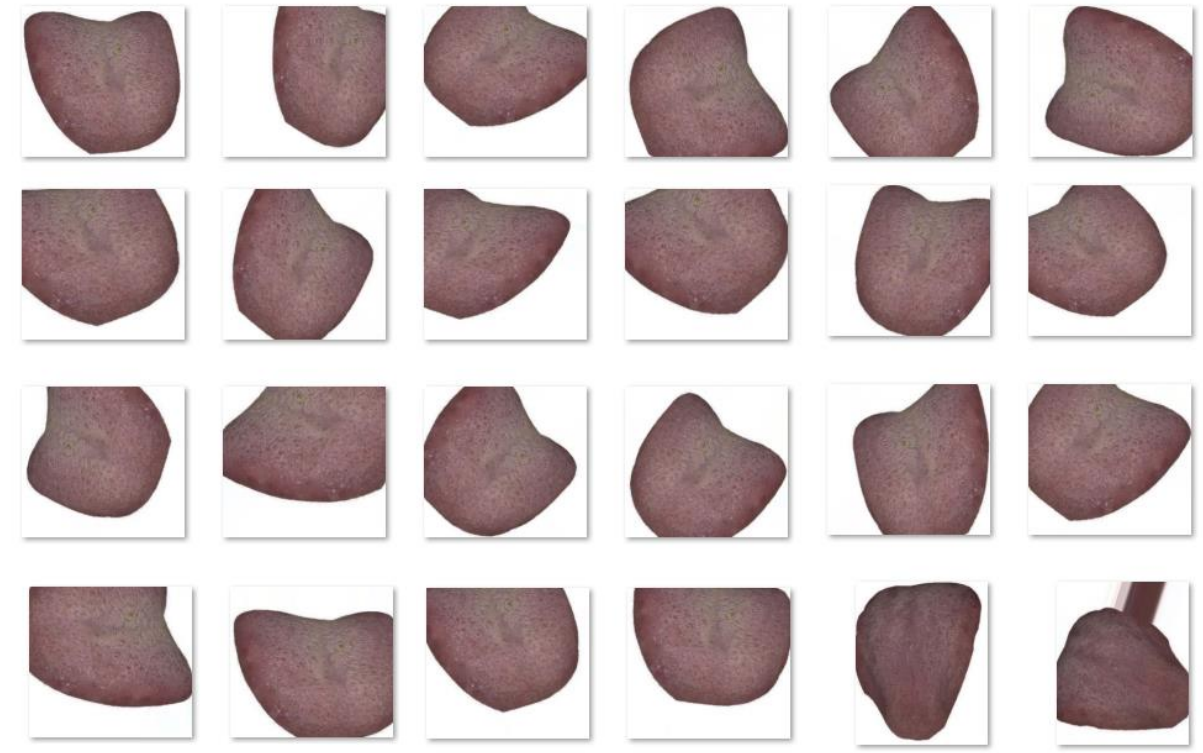

Fig. 3. Sample Tongue Images

Fig. 4 visualizes the results of the presented preprocessing stage. Fig. 4a& 4c shows the input original tongue images and Fig. 4b & 4d depicts the preprocessed versions.

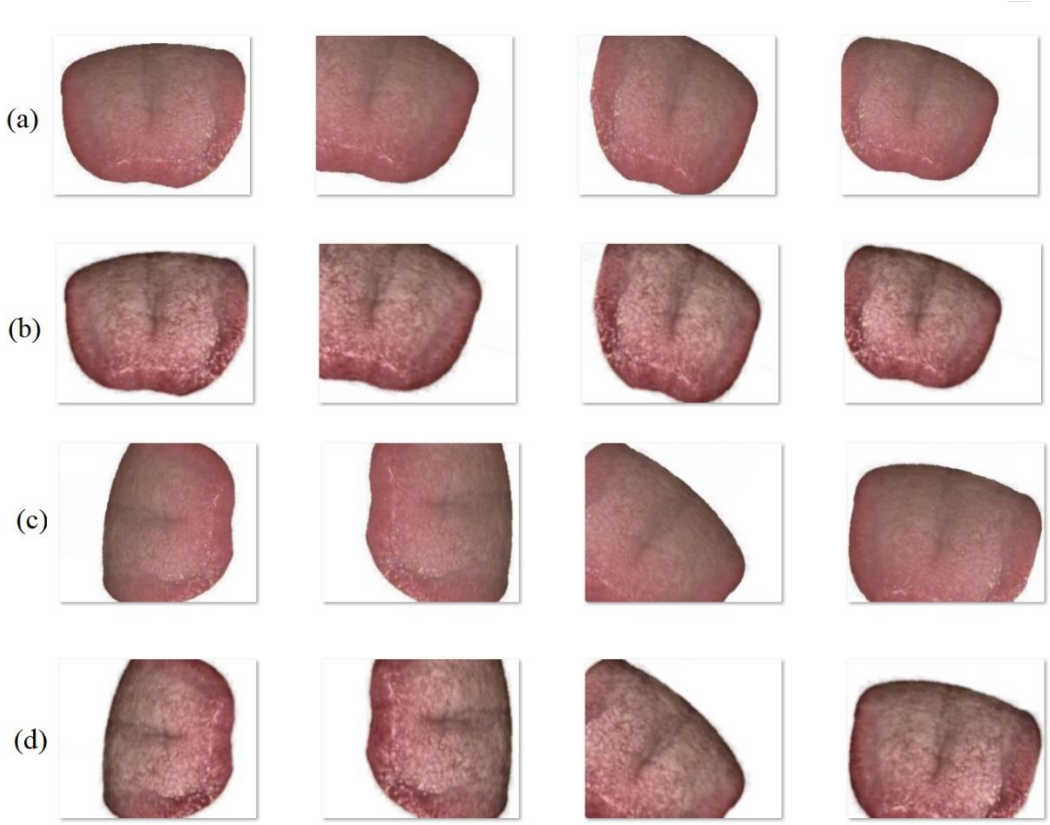

Fig. 4. a and c) Original Image b and d) Preprocessed Image

Fig. 5 illustrates the confusion matrix created by the presented VGG19-GNB model. The figure reported that the VGG19-GNB model has effectively classified 73 images under CB class, 65 images under CCCI class, 78 images under CKD class, 77 images under CHD, 66 images under EG class, 78 images under healthy class, 77 images under MH class, 67 images under NS class, 66 images under NH class, 65 images under PN class, 78 images under URTI class, and 76 images under VG class.

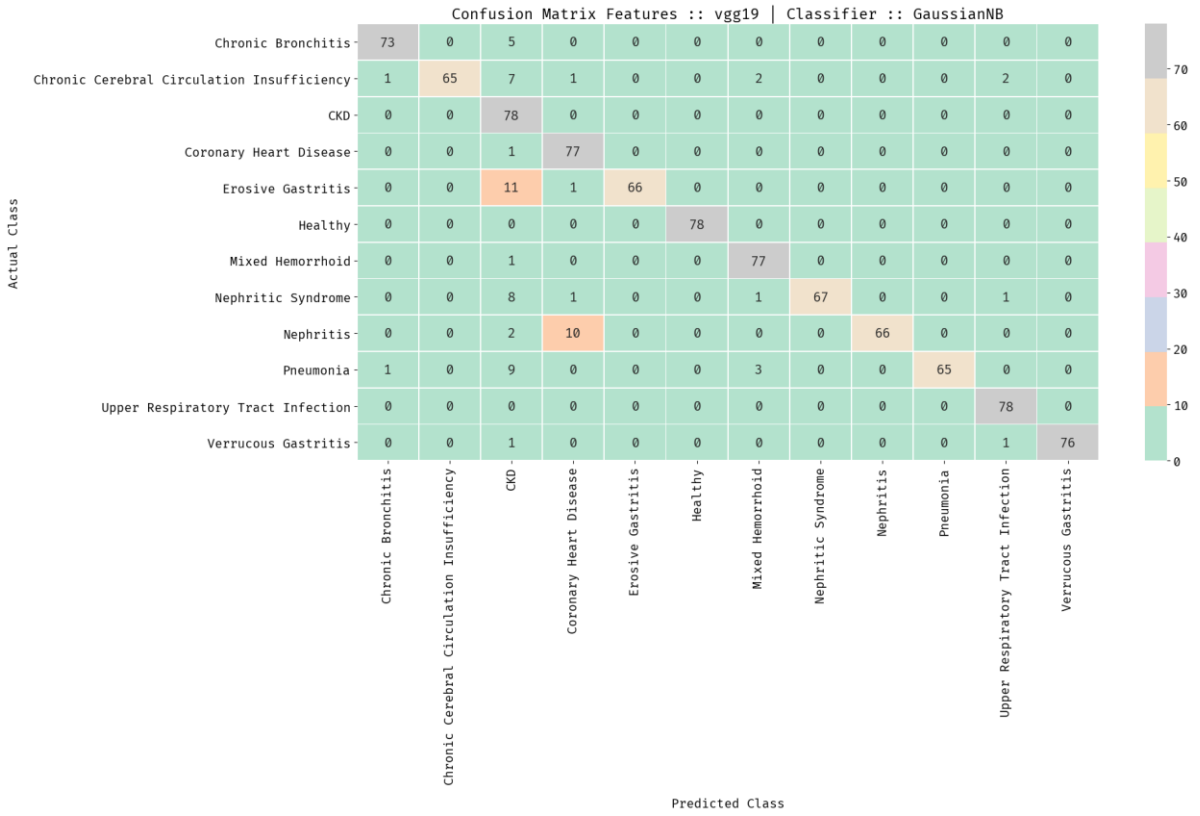

Fig. 5. Confusion Matrix of VGG19-GNB

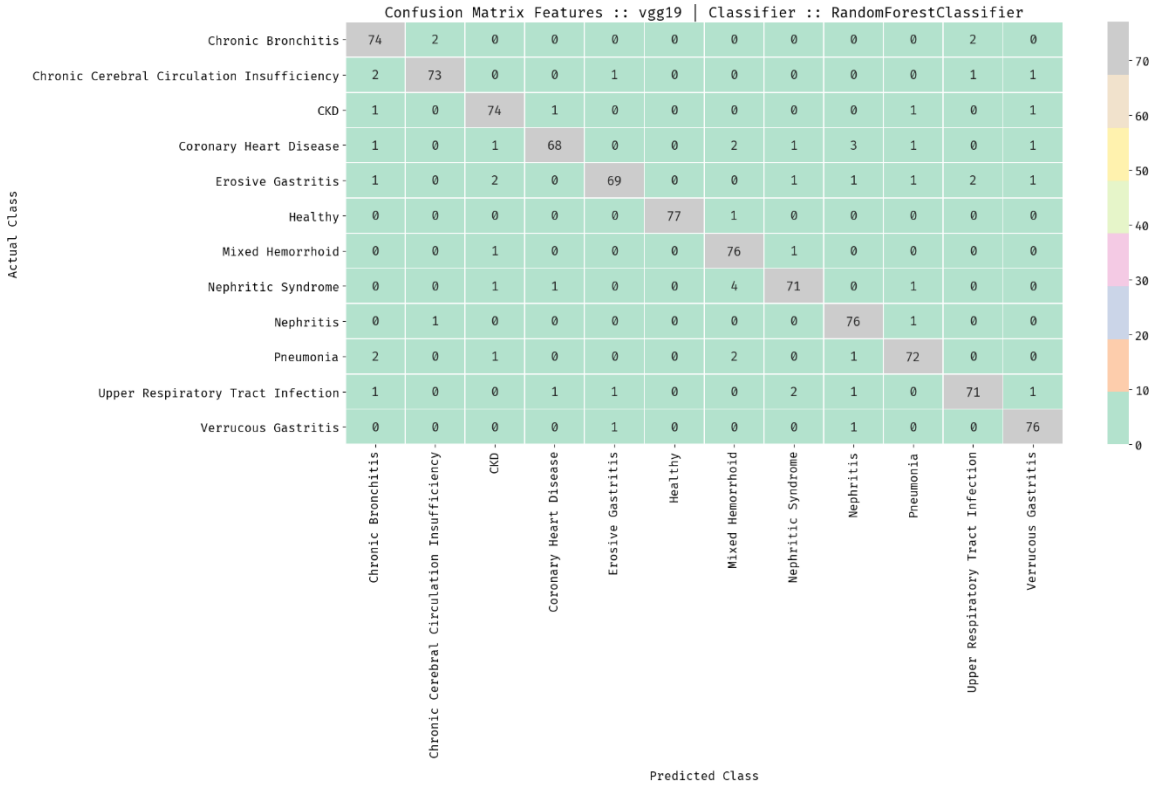

Fig. 6. Confusion Matrix of VGG19-RF

Fig. 6 illustrates the confusion matrix created by the presented VGG19-RF model. The figure reported that the VGG19-RF model has effectively classified 74 images under CB class, 73

images under CCCI class, 74 images under CKD class, 68 images under CHD, 69 images under EG class, 77 images under healthy class, 76 images under MH class, 71 images under NS class, 76 images under NH class, 72 images under PN class, 71 images under URTI class, and 76 images under VG class.

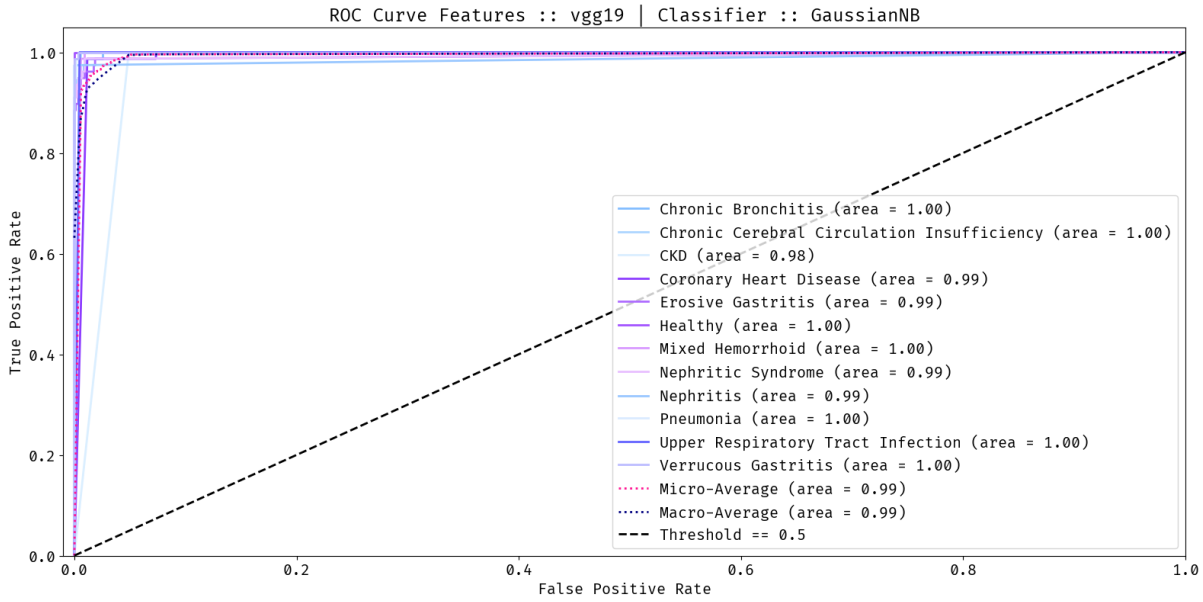

Fig. 7. ROC Analysis of VGG19-GNB

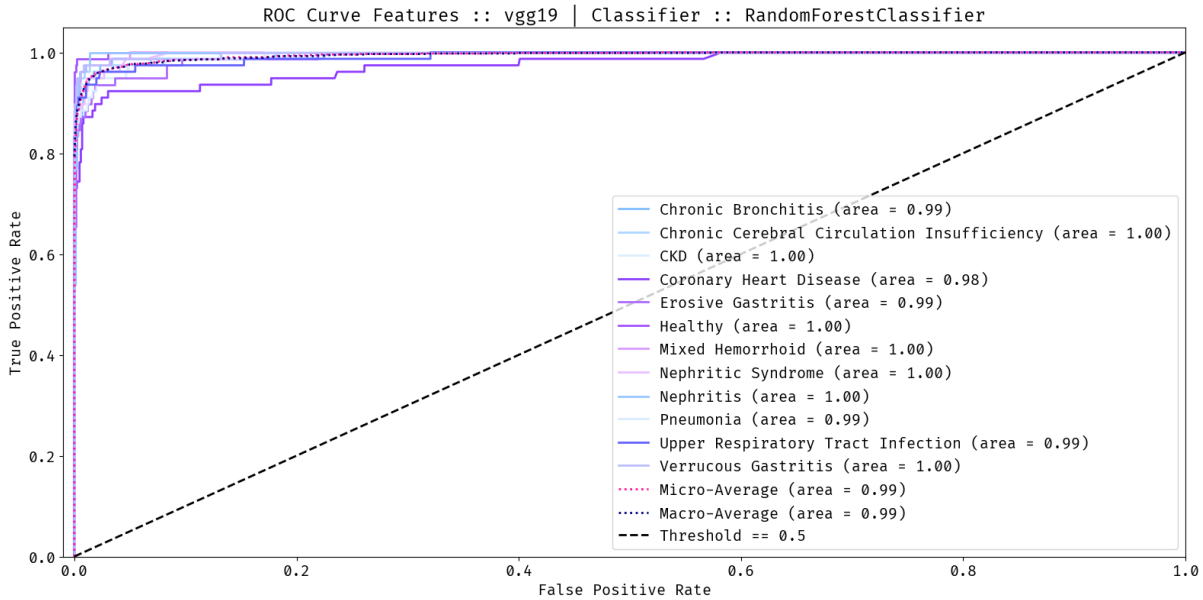

Fig. 8. ROC Analysis of VGG19-RF

Fig. 7 shows the ROC analysis of the VGG19-GNB model on the classification of tongue images. The figure showcased that the VGG19-GNB model has resulted in superior classification performance and attained better ROC value on all the applied class labels.Fig. 8 shows the ROC analysis of the VGG19-RF model on the classification of tongue images. The figure showcased that the VGG19-RF model has resulted in superior classification performance and attained better ROC value on all the applied class labels.

Table 2 and Figs. 9-10 demonstrates the classification performance analysis of the four proposed models. The table values signified that the presented VGG19-GNB model has attained better classification performance over the compared methods. Firstly, the VGG19-RF model has obtained effective classification with the precision of 93.8%, recall of 93.7%, accuracy of 93.7%, and F1-score of 93.68%. At the same time, the VGG19-GNB approach has achieved effective classification with a precision of 94.52%, recall of 92.52%, accuracy of 92.52%, and F1-score of 92.84%.

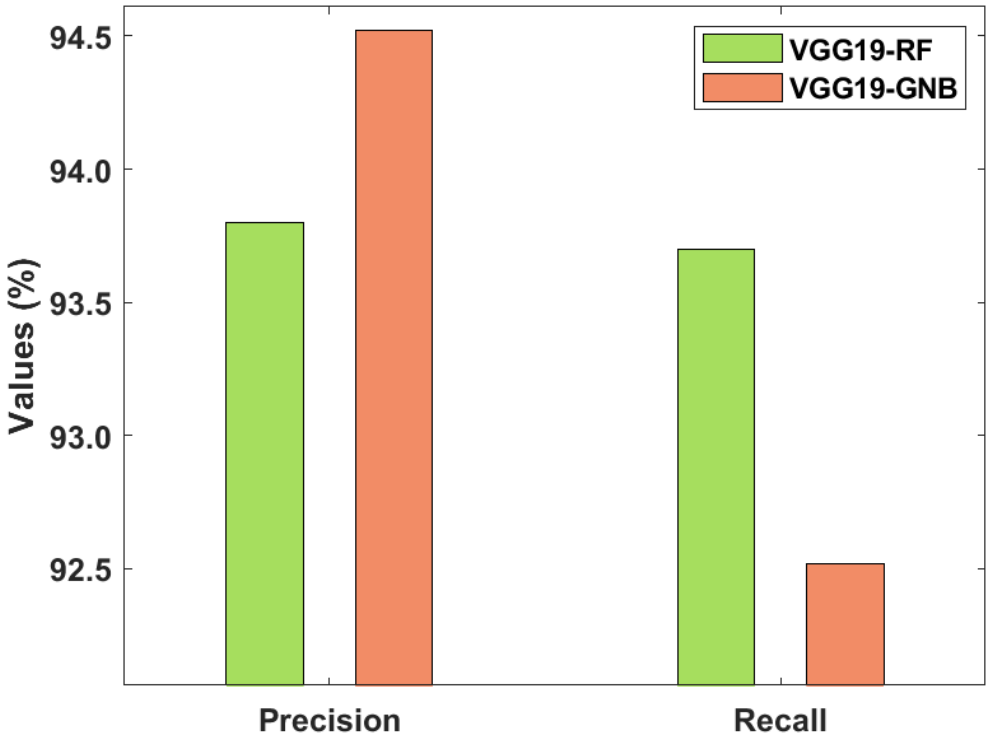

Fig. 9. Precision and recall analysis of proposed method

Table 2 Performance Analysis of Proposed Methods in terms of Different Measures

Methods	**Precision**	**Recall**	**Accuracy**	**F1-Score**
VGG19-RF	93.80	93.70	93.70	93.68
VGG19-GNB	94.52	92.52	92.52	92.84

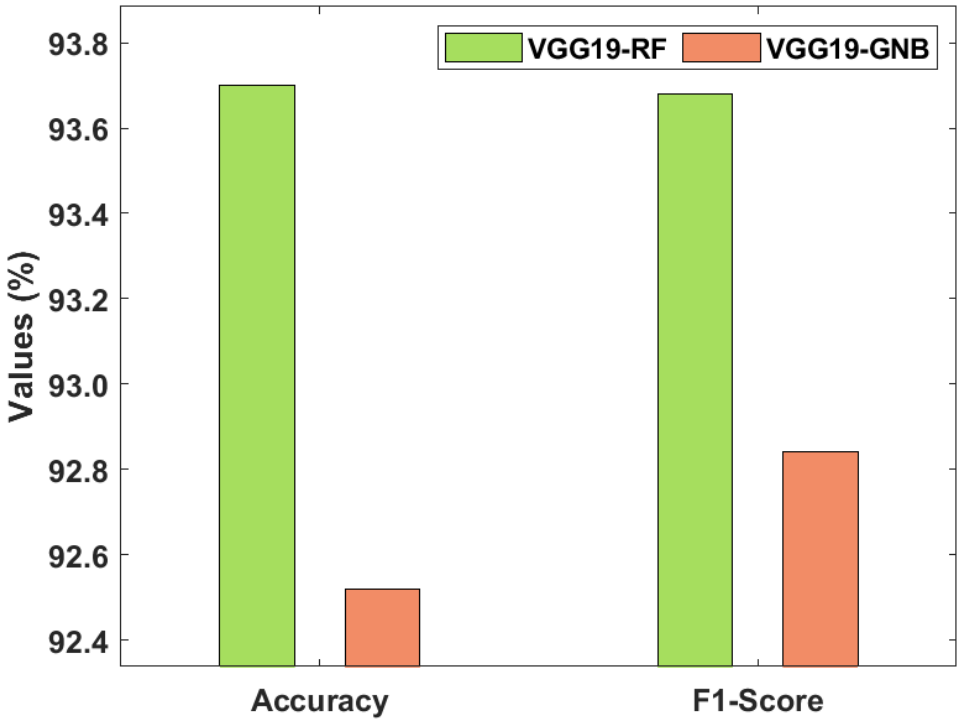

Fig. 10. Accuracy and F1-score analysis of proposed method

Table 3 and Fig. 11 offers a comprehensive comparative results analysis with the recent state of art methods [16-22] such as Geometry Features+Sparse Representation Classifier (GF+SRC), Conceptual Alignment Deep Autoencoder (CADAE), KNN, GA-SVM, SVM, and VGG-SVM. The figure has shown that the VGG-SVM model has depicted ineffective classifier results with the minimal accuracy of 59.44%. At the same time, the KNN model has tried to accomplish slightly better results over the VGG-SVM model with an accuracy of 73.38%. Also, the Bayesian, Geometry features, SVM, and CADAE models have depicted moderate and closer accuracy values of 75%, 76.24%, 76.46%, and 77%.

Table 3 Performance Analysis of Proposed Methods with Existing Methods in terms of Different Measures

Methods	**Accuracy**
Proposed VGG19-RF	93.70
Proposed VGG19-GNB	92.52
Geometry Features	76.24
Bayesian	75.00
K-NN	73.38
SVM	76.46
GA-SVM	83.06

VGG-SVM	59.44
GF+SRC	79.23
CADAE	77.00

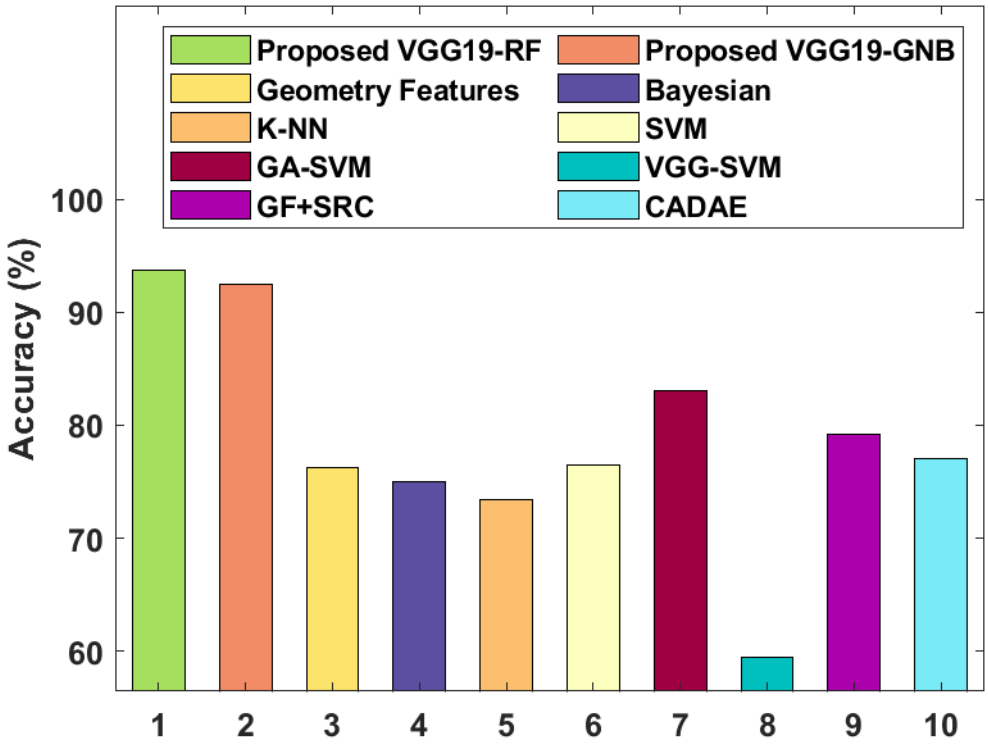

Fig. 11. Accuracy analysis of proposed method with existing methods

Additionally, GF+SRC model has reached a slightly higher accuracy value of 79.23%. Also, the GA-SVM model has demonstrated that even better result with accuracy of 83.06%. But, the proposed VGG19-RF and VGG19-GNB models have showcased that attained maximum results with accuracy of 93.7% and 92 .52%. The experimental values pointed out that the presented VGG19-RF model has reached a higher precision, recall, accuracy, and F1-Score of 93.80%, 93.70%, 93.70%, and 93.68% respectively.

4. Conclusion:

This paper has devised a new automated DL based tongue color image analysis for disease diagnosis and classification. During the preprocessing stage, the presented model utilizes data augmentation for increasing the size of the training dataset and GF technique for noise removal. Then, the VGG-19 model gets executed to derive a useful set of feature vectors. Subsequently, the GNB and RF models are applied to categorize the distinct class labels of the applied test images. For evaluating the classification results of the presented model, benchmark tongue image dataset is used. The experimental values pointed out that the presented VGG19-RF model has reached a higher precision, recall, accuracy, and F1-Score of 93.80%, 93.70%, 93.70%, and 93.68% respectively. In future, the presented model can be extended by the use of advanced DL architectures in place of VGG-19 model.

References:

[1] Y. Jiao, X. Zhang, L. Zhuo, M. Chen, and K. Wang, "Tongue image classification based on Universum SVM," in Proceedings of the 3rd International Conference on BioMedical Engineering and Informatics (BMEI '10), pp. 657–660, IEEE, Yantai, China, October 2010.

[2] Y.-G. Wang, J. Yang, Y. Zhou, and Y.-Z. Wang, "Region partition and feature matching based color recognition of tongue image," Pattern Recognition Letters, vol. 28, no. 1, pp. 11–19, 2007.

[3] X. Wang, B. Zhang, Z. Yang, H. Wang, and D. Zhang, "Statistical analysis of tongue images for feature extraction and diagnostics," IEEE Transactions on Image Processing, vol. 22, no. 12, pp. 5336–5347, 2013

[4] G. Cao, J. Ding, Y. Duan, L. Tu, J. Xu, and D. Xu, "Classification of tongue images based on doublet and color space dictionary," in Proceedings of the IEEE International Conference on Bioinformatics and Biomedicine (BIBM '16), Shenzhen, China, December 2016.

[5] Z. Guo, "Tongue image matching using color and texture," in Proceedings of the International Conference on Medical Biometrics (ICMB '08), pp. 273–281, Hong Kong, 2008.

[6] B. Pang, D. Zhang, and K. Wang, "Tongue image analysis for appendicitis diagnosis," Information Sciences, vol. 175, no. 3, pp. 160–176, 2005.

[7] X. Zhang, J. Zhang, G. Hu, and Y. Wang, "Preliminary study of tongue image classification based on multi-label learning," in Advanced Intelligent Computing Theories and Applications, vol. 9227 of Lecture Notes in Computer Science, pp. 208–220, Springer, 2015.

[8] T.-H. Chan, K. Jia, S. Gao, J. Lu, Z. Zeng, and Y. Ma, "PCANet: a simple deep learning baseline for image classification?" IEEE Transactions on Image Processing, vol. 24, no. 12, pp. 5017–5032, 2015.

[9] Nandan, D., Kanungo, J. and Mahajan, A., 2018. An error-efficient Gaussian filter for image processing by using the expanded operand decomposition logarithm multiplication. Journal of ambient intelligence and humanized computing, pp.1-8.

[10] Islam, M.Z., Islam, M.M. and Asraf, A., 2020. A combined deep CNN-LSTM network for the detection of novel coronavirus (COVID-19) using X-ray images. Informatics in Medicine Unlocked, 20, p.100412.

[11] Mateen, M., Wen, J., Song, S. and Huang, Z., 2019. Fundus image classification using VGG-19 architecture with PCA and SVD. Symmetry, 11(1), p.1.

[12] https://www.kaggle.com/keras/vgg19/home

[13] Tahmassebi, A., Gandomi, A.H., Schulte, M.H., Goudriaan, A.E., Foo, S.Y. and Meyer-Baese, A., 2018. Optimized naive-bayes and decision tree approaches for fmri smoking cessation classification. Complexity, 2018.

[14] L. Breiman, "Random forests," Machine Learning, vol. 45, no. 1, pp. 5–32, 2001.

[15] Gao, X., Wen, J. and Zhang, C., 2019. An improved random forest algorithm for predicting employee turnover. Mathematical Problems in Engineering, 2019.

[16] Zhang, B. and Zhang, H., 2015. Significant geometry features in tongue image analysis. Evidence-based Complementary and Alternative Medicine: eCAM, 2015.

[17] Tania, M.H., Lwin, K. and Hossain, M.A., 2019. Advances in automated tongue diagnosis techniques. Integrative Medicine Research, 8(1), pp.42-56.

[18] Zhang, B., Wang, X., You, J. and Zhang, D., 2013. Tongue color analysis for medical application. Evidence-Based Complementary and Alternative Medicine, 2013.

[19] Zhang, J., Xu, J., Hu, X., Chen, Q., Tu, L., Huang, J. and Cui, J., 2017. Diagnostic method of diabetes based on support vector machine and tongue images. BioMed Research International, 2017.
[20] Ma, J., Wen, G., Hu, Y., Chang, T., Zeng, H., Jiang, L. and Qin, J., 2018. Tongue image constitution recognition based on Complexity Perception method. arXiv preprint arXiv:1803.00219.
[21] Zhang, H. and Zhang, B., 2014, May. Disease detection using tongue geometry features with sparse representation classifier. In 2014 International Conference on Medical Biometrics (pp. 102-107). IEEE.
[22] Balu, S. and Jeyakumar, V., 2020. A Study on Feature Extraction and Classification for Tongue Disease Diagnosis. In Intelligence in Big Data Technologies—Beyond the Hype (pp. 341-351). Springer, Singapore.

Appendix

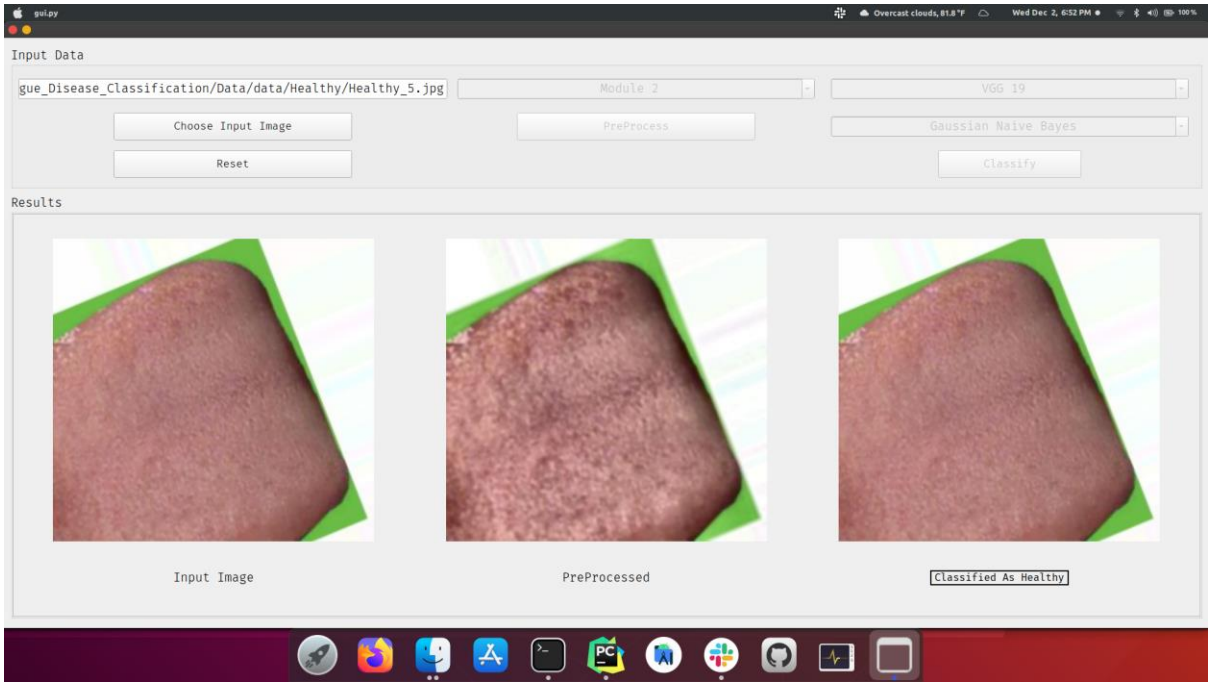

Classification Result of Healthy Image

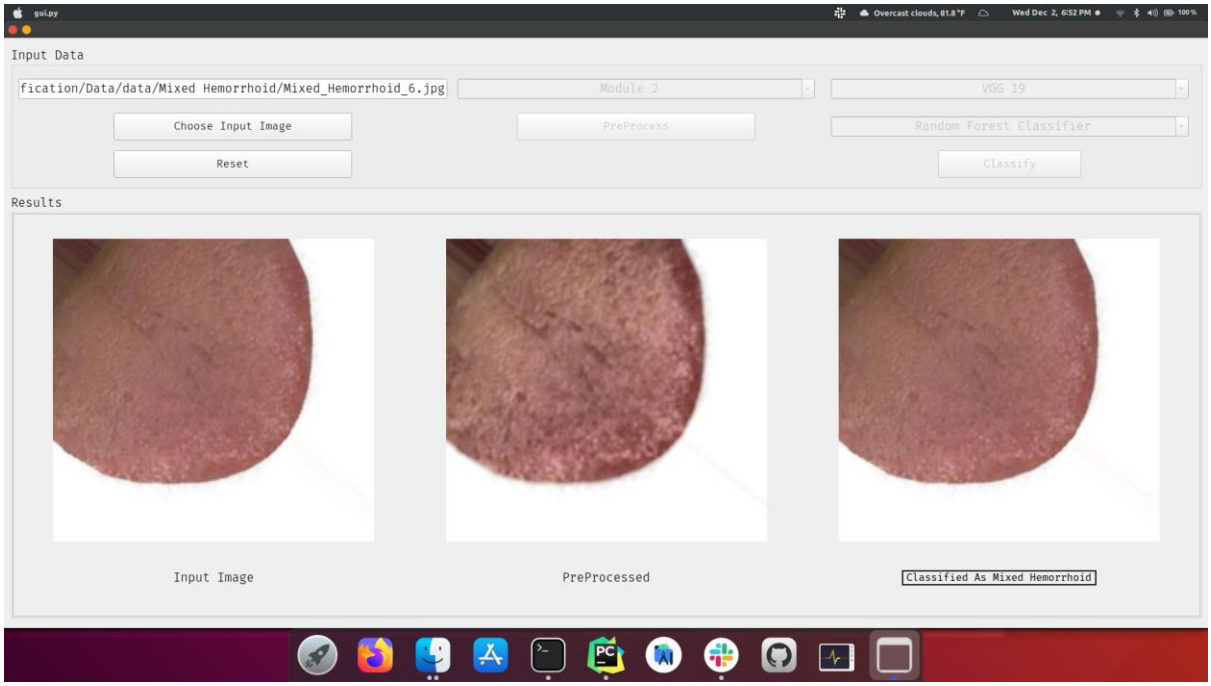

Classification Result of Hemorrhoid Image